remote sensing

MDPI

Article

Forest Fire Spread Monitoring and Vegetation Dynamics Detection Based on Multi-Source Remote Sensing Images

Yuping Tian, Zechuan Wu, Mingze Li *,†, Bin Wang † and Xiaodi Zhang

Key Laboratory of Sustainable Forest Ecosystem Management-Ministry of Education, School of Forestry, Northeast Forestry University, Harbin 150040, China
* Correspondence: mingzelee@nefu.edu.cn
† These authors contributed equally to this work.

Abstract: With the increasingly severe damage wreaked by forest fires, their scientific and effective prevention and control has attracted the attention of countries worldwide. The breakthrough of remote sensing technologies implemented in the monitoring of fire spread and early warning has become the development direction for their prevention and control. However, a single remote sensing data collection point cannot simultaneously meet the temporal and spatial resolution requirements of fire spread monitoring. This can significantly affect the efficiency and timeliness of fire spread monitoring. This article focuses on the mountain fires that occurred in Muli County, on 28 March 2020, and in Jingjiu Township on 30 March 2020, in Liangshan Prefecture, Sichuan Province, as its research objects. Multi-source satellite remote sensing image data from Planet, Sentinel-2, MODIS, GF-1, GF-4, and Landsat-8 were used for fire monitoring. The spread of the fire time series was effectively and quickly obtained using the remote sensing data at various times. Fireline information and fire severity were extracted based on the calculated differenced normalized burn ratio (dNBR). This study collected the meteorological, terrain, combustibles, and human factors related to the fire. The random forest algorithm analyzed the collected data and identified the main factors, with their order of importance, that affected the spread of the two selected forest fires in Sichuan Province. Finally, the vegetation coverage before and after the fire was calculated, and the relationship between the vegetation coverage and the fire severity was analyzed. The results showed that the multi-source satellite remote sensing images can be utilized and implemented for time-evolving forest fires, enabling forest managers and firefighting agencies to plan improved firefighting actions in a timely manner and increase the effectiveness of firefighting strategies. For the forest fires in Sichuan Province studied here, the meteorological factors had the most significant impact on their spread compared with other forest fire factors. Among all variables, relative humidity was the most crucial factor affecting the spread of forest fires. The linear regression results showed that the vegetation coverage and dNBR were significantly correlated before and after the fire. The vegetation coverage recovery effects were different in the fire burned areas depending on fire severity. High vegetation recovery was associated with low-intensity burned areas. By combining the remote sensing data obtained by multi-source remote sensing satellites, accurate and macro dynamic monitoring and quantitative analysis of wildfires can be carried out. The study's results provide effective information on the fires in Sichuan Province and can be used as a technical reference for fire spread monitoring and analysis through remote sensing, enabling accelerated emergency responses.

Keywords: multi-source remote sensing; forest fire; forest fire monitor; vegetation recovery; forest fire factors

Citation: Tian, Y.; Wu, Z.; Li, M.; Wang, B.; Zhang, X. Forest Fire Spread Monitoring and Vegetation Dynamics Detection Based on Multi-Source Remote Sensing Images. *Remote Sens.* **2022**, *14*, 4431. https://doi.org/10.3390/rs14184431

Academic Editors: Eben Broadbent, Robert Treuhaft, Fabio Gonçalves and André Almeida

Received: 13 July 2022
Accepted: 2 September 2022
Published: 6 September 2022

1. Introduction

As an important material basis for the country's sustainable development, forests are vital and renewable resources in economic and ecological environment construction [1]. In particular, forests have a huge carbon sequestration function and play an important

role as a buffer for climate change and maintaining ecological security [2,3]. However, forest ecosystems often suffer from various human and natural disturbances, including forest pests and diseases, multiple fires, and artificial logging [4–6]. Forest fire is a natural disaster with such strong suddenness and destructive power that it is not easy to rescue the forests. Forest fires damage the structure, composition, and function of virgin forests to a certain extent, and can even threaten the safety of human beings and affect the region's carbon cycle in severe cases. Forest fires are severe natural disasters that threaten human security, wildlife habitat, regional economies, and global climate change [7–10]. Reducing fire occurrence and damage has become one of the cornerstone tasks of protecting ecological resources [11,12].

Traditionally, mechanical equipment and artificial environment monitoring are used to track the spread of forest fires and extract information about burned areas [13]. However, transportation issues make measuring fires in remote areas and steep terrains more difficult. In addition, manual monitoring is a very dangerous and costly resource [14,15]. With the continuous development of remote sensing technologies, the emergence of remote sensing images with higher spatial, temporal, and radiometric resolution provides many reliable data sources for forest fire monitoring. At the same time, the rapid and accurate extraction of the fire location, area, progression, and other information hidden in remote sensing images play an essential role in improving the monitoring effect [16]. The Landsat series satellites, developed and launched by the National Aeronautics and Space Administration (NASA), are characterized by rich spectral information and medium resolution. They can better identify the areas burned by fire and have advantages in forest fire monitoring [17]. However, continuous time series images cannot be obtained due to time resolution limitations of up to 16 days. There is an increased interest in the monitoring ability of the binary star system (Aqua and Terra) of the Moderate Resolution Imaging Spectroradiometer (MODIS) image to the exact location and the unique induction of the band to the fire point, which has significantly improved our ability to observe fire spread [18]. MODIS has a sensitive fire detection channel, which can support qualitative and quantitative analysis of areas burned by forest fire etc. In this way, it plays an important role in enhancing the visual expression of the forest fire environment and accurately identifying fire points. MODIS records four images daily, which can monitor the incidence of a forest fire in a timely and effective manner [19]. However, due to the fact that the spatial resolution of the band used for fire monitoring is 500 m, it is difficult to effectively monitor the spread of small fires. Sentinel 2 is a high-resolution multispectral imaging satellite composed of Sentinel-2A and Sentinel-2B satellites. The Sentinel-2 satellite covers 13 spectral bands with ground resolutions of 10 m, 20 m, and 60 m and provides red-edge spectral bands [20]. The emergence of the GaoFen (GF) series images has resulted in their being widely used in meteorology, forest fire monitoring, earthquake relief, and in other fields. They also have great potential in forest fire early warning and prediction applications, further enhancing the ability of satellite forest fire monitoring [21]. GF-1 data has high temporal and spatial resolution characteristics, it is easy to obtain time-series images, and the spatial resolution is 16 m [22]. The GF-4 is China's first civilian satellite in geosynchronous orbit, with a high spatial resolution. In addition, as a geostationary orbiting meteorological satellite, the same area images in a sequence can be obtained within a few minutes. Since the GF-4 satellite has such high resolution, it is an indispensable remote sensing data source for fire spread monitoring [21]. Planet satellite has been an emerging remote sensing satellite in recent years. It is also the only remote sensing satellite in the world with a global high resolution, high frequency, and full coverage capability. It has good image quality, high data coverage efficiency, and a 3–5 m spatial resolution. The Planet constellation has more than 170 satellites, and hundreds of satellites take images around the world daily, achieving global daily coverage [23].

Remote sensing technologies have become one of the most used fire occurrence and monitoring tools. Compared with traditional ground observations, remote sensing images have a high imaging temporal frequency, and a wide comprehensive monitoring range

and are sensitive to the thermal radiation of forest fires [24–26]. After a fire occurs, remote sensing data from a single satellite cannot meet the requirements of time and space resolution at the same time, so it is difficult to meet the emergency needs of monitoring fire and fire location [27,28]. Furthermore, a single monitoring result may be constrained by environmental factors, such as bad weather, which reduces monitoring effectiveness and makes it impossible to collect reliable, detailed fire data or carry out firefighting operations [29]. Currently, because of the shortcomings of a single remote sensing observation time, several studies have been using various remote sensing satellite monitoring data to increase the observation frequency of satellites. Good results have been obtained for forest resource inventory using multi-source remote sensing data and for assessing forest structure changes along productivity gradients after fires in the Canadian boreal forests [30,31]. In addition, multi-source satellite products were used to assess the characteristics of major recent wildfires in the United States, Australia, and Brazil in 2018–2019, with satisfactory results [32]. For example, the object-oriented analysis method is used to dynamically monitor the fire burned area based on multiple remote sensing image data, or machine learning techniques, such as Long Short Term Memory (LSTM) and Fuzzy logic models, are utilized, which can overcome the shortcomings of the small number of images and data acquired by a single satellite so as to better and continuously monitor the fire burned area [33,34]. Using spectral indicators, such as the normalized differenced vegetation index (NDVI) and the fire burned area identification index, a time series identification of fire regions on remote sensing satellite images can be obtained by Landsat and GF series satellites [35,36]. When monitoring and obtaining the fire burned areas, some methods using the thresholds and spectral indices have achieved good results [37–39]. Therefore, the advantages of different remote sensing data should be fully considered, and multi-source remote sensing data should be coordinated to obtain fire occurrence and area information from different sources and forms of remote sensing information quickly, accurately, with high quality and efficiency to improve fire monitoring accuracy and timeliness. Achieving regular and even real-time monitoring of forest resources provides an important basis for forest fire monitoring and forest inventory and resource protection. There are few research studies and applications of fire spread monitoring combined with various high, medium and low-resolution remote sensing satellite image data, especially applications based on high-resolution Planet satellites.

This study aims to provide a scientific basis for fire prevention and fighting, fire trend inversion and disaster loss reduction. Therefore, utilizing data from the fires in Sichuan Province, this paper combines the advantages of multi-source remote sensing satellites to extract the time series of spreading fire lines to acquire the location and time evolution of the fire. This approach can accurately calculate and analyze the area and how it changed at different times after the fire. It can calculate and classify the fire intensity and quantitatively analyze the dynamic changes in the vegetation in the study area before and after the fire. Combining three different types of remote sensing data of low, medium, and high resolution can accurately and quickly judge the direction of fire spread and solves the problem that single remote sensing data cannot be continuously monitored. It provides approaches to further explore the ability to use multiple remote sensing satellite image data to collaborate in monitoring the spread of fires and construct forest fire assessment techniques based on different spatiotemporal image data. It ultimately provides a scientific and reasonable technical system for forest fire monitoring and prevention.

The rest of this paper is organized as follows. A collection of multi-source remote sensing data and forest fire factors, and detailed description of experimental methods, is presented in Section 2. In Section 3, based on the multi-source remote sensing data of two forest fires in Sichuan Province, the burned area of the time series was extracted, a forest fire factor importance experiment was conducted and forest fire intensity grade and vegetation coverage experimental analysis were carried out. Sections 4 and 5 discuss the results and some prospects for future work.

2. Materials and Methods

2.1. Study Area

This study focused on the mountain fires that occurred in Muli County, on 28 March 2020, and Jingjiu Township, on 30 March 2020 in Liangshan Prefecture, Sichuan Province, China (Figure 1). The Muli County is located northwest of Liangshan between 100°03′~101°40′E and 27°40′~29°10′N. At 19:00 p.m. on 28 March 2020, a mountain fire broke out in Muli County, Sichuan Province. The fire lasted nine days until April 5, when the open flames and smoke points were extinguished. The average altitude of the fire site was 4000 m, with Pinus yunnanensis and shrubs mainly covering the area. The Jingjiu Township is located in the south-central part of Xichang city, Sichuan Province, between 101°46′~102°25′E and 27°32′~28°10′N. At 15:00 p.m. on 30 March 2020, a fire broke out in Jingjiu Township, Sichuan Province. By 2 April, all the fires were extinguished. The average altitude of the fire site is 1800 m, and Ageratina adenophora and shrubs dominate the surface vegetation. Since the beginning of spring in 2020, southwest China has experienced drought and less rain, with significantly higher temperatures and more windy weather. In the Liangshan area, it was especially sunny in March, with a high temperature, no rainfall for 20 consecutive days, and a humidity of less than 10%. Due to the extreme weather, complex terrain, steep slope, and inconvenient traffic communication, fire emergency monitoring and firefighting faced great difficulties.

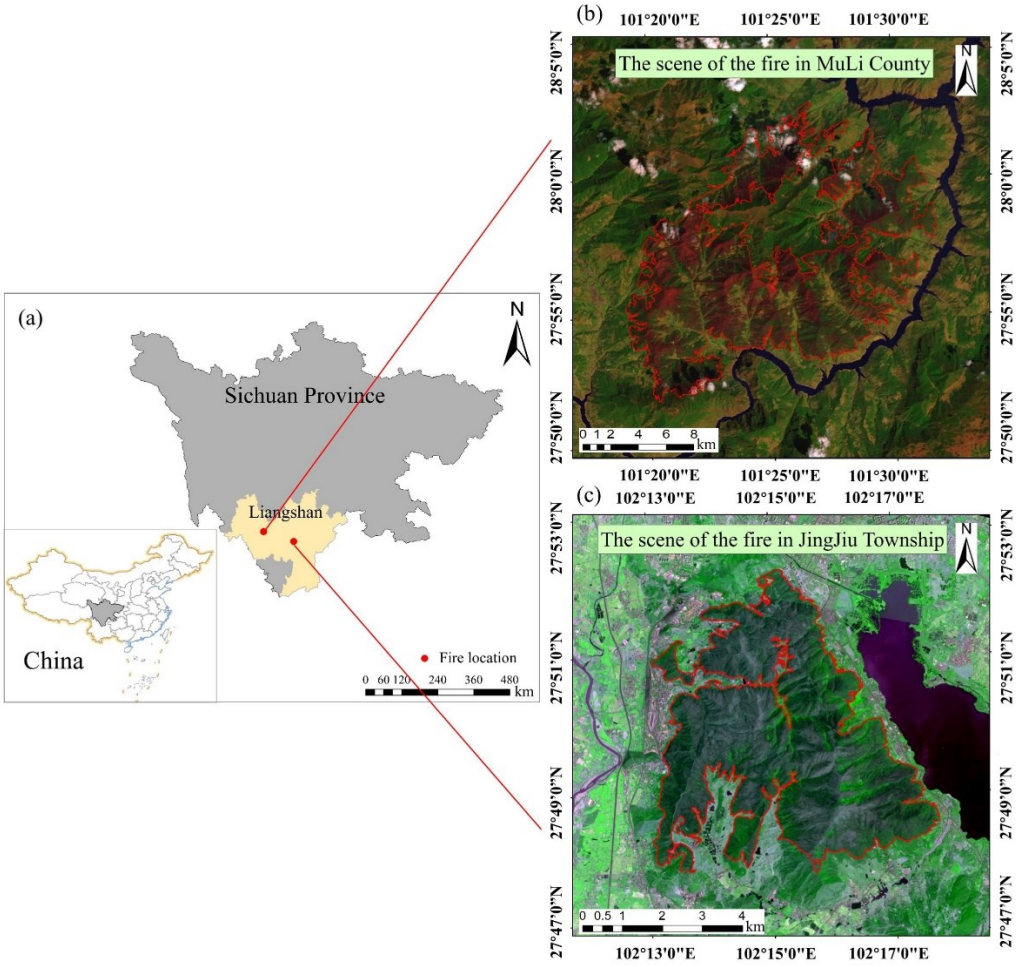

Figure 1. Location of the study area and the fire site. (**a**) the location of the study area, (**b**) the scene of the fire in MuLi County, (**c**) the scene of the fire in JingJiu Township.

2.2. Remote Sensing Data

After the fire, satellite image data from multiple satellites were used for fire monitoring. The multiple remote sensing satellite images acquired by the Planet, Sentinel-2, Landsat-8, GF-1, GF-4, and MODIS satellites, the fire front, and the burned area were monitored in this study. A total of 29 images were obtained with the specific data information shown in Table 1.

Table 1. Selected remote sensing datasets.

Data Type	Acquisition Date	Acquisition Time	Spatial Resolution	Source
Planet	1 April 2020 10 April 2020	11:01 11:30	3 m	Planet Lab www.planet.com/explorer/ (accessed on 6 January 2022)
Sentinel-2	30 March 2020 20 March 2020	11:45 11:46	10 m	
Landsat 8	13 March 2020 5 April 2020 16 May 2020 28 February 2021 23 March 2021	11:40 11:46 11:39 11:40 11:46	30 m	Geospatial Data Cloud www.gscloud.cn/ (accessed on 14 January 2022)
GF-1	30 March 2020	12:30	16 m	China Centre For Resources Satellite Data and Application www.cresda.com/CN/ (accessed on 2 February 2022)
GF-4	31 March 2020 1 April 2020 29 March 2020	11:47; 13:38; 14:55; 15:00; 16:41 11:52; 14:14; 15:17 12:45	50 m/400 m	
MODIS	30 March 2020 31 March 2020 1 April 2020 5 April 2020	11:50; 13:20 10:55; 12:30; 14:05; 14:06 11:35; 11:45; 13:10 11:10	500 m	EARTHDATA ladsweb.modaps.eosdis.nasa.gov/search/ (accessed on 11 February 2022)

Each remote sensing image (Planet, Sentinel-2, Landsat 8, GF-1, MODIS) obtained was used to extract the burned area, including Landsat-8 satellite to extract the fire intensity and vegetation fractional coverage (*VFC*), GF-4 satellite to locate the fire and monitor the dynamic time series of the fire. The monitoring process is shown in Figure 2.

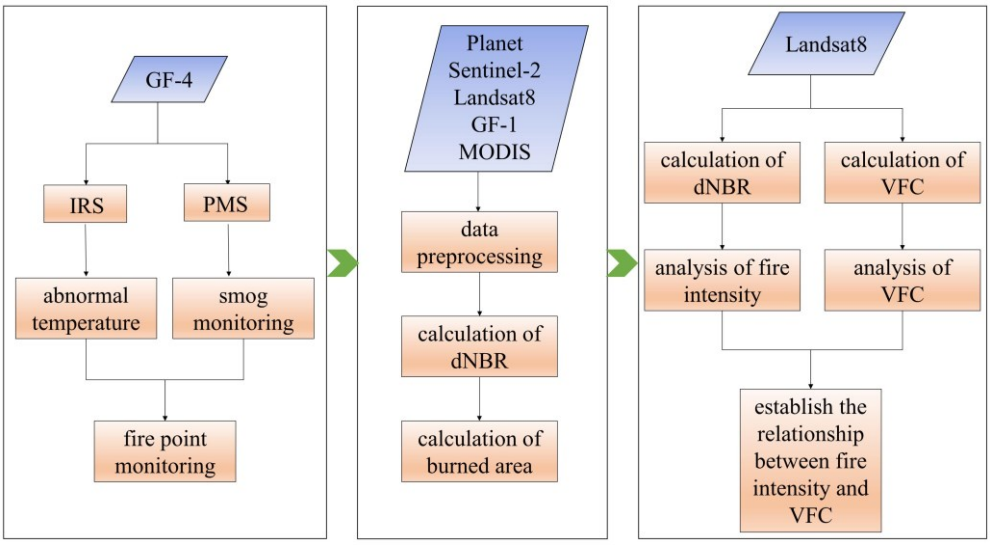

Figure 2. Flow chart of forest fire monitoring with multi-source remote sensing data.

During the processing of satellite remote sensing images, various radiometric errors and geometric deformations occur [40,41]. When selecting the image, the image with no

cloud or less cloud cover should be selected as far as possible. If the image has clouds, the cloud mask algorithm should be used for cloud removal. According to the actual situation of remote sensing images in this study, radiometric calibration, atmospheric correction and geometric correction were preprocessed. Due to the different spatial resolutions of each data source, all data were resampled to 3 m in this study and then information was extracted.

Among them, the GF4 satellite IRS was used to observe the abnormally high fire temperature, and the PMS monitored the smoke and the fire point. The converted IRS data could detect abnormal temperatures on the ground. By radiometric calibration, the remote sensing image *DN* value could be converted into a radiation value to achieve temperature conversion. The equation is described as follows:

$$L_e(\lambda_i) = Gain \cdot DN + offset \quad (1)$$

where $L_e(\lambda_i)$ denoted the converted radiance value ($W \cdot m^{-2} \cdot sr^{-1} \cdot um^{-1}$), λ_i was the central wavelength of channel *i*, *DN* denoted the observed load, *Gain* represented the calibration slope ($W \cdot m^{-2} \cdot sr^{-1} \cdot um^{-1}$), and *offset* was the offset of the absolute calibration coefficient ($W \cdot m^{-2} \cdot sr^{-1} \cdot um^{-1}$). In this study, *Gain* was 0.01107 $W \cdot m^{-2} \cdot sr^{-1} \cdot um^{-1}$, and *offset* was -0.878625 $W \cdot m^{-2} \cdot sr^{-1} \cdot um^{-1}$.

After the above conversion, the temperature was calculated using the Planck function. The equation is described as follows:

$$T_i = \frac{K_{i2}}{\ln(1 + K_{i1}/L_e(\lambda_i))} \quad (2)$$

where K_{i1} and K_{i2} were constants, $K_{i1} = 2h \cdot c^2/\lambda_i^5$, $K_{i2} = h \cdot c/(k \cdot \lambda_i)$, h represented the Planck constant, which was about 6.6261×10^{-34} J·s, c denoted the light speed, which was about 2.9979×10^8 m/s, and k stood for the Boltzmann constant, which was about 1.3807×10^{-23} $J \cdot K^{-1}$.

2.3. Forest Fire Factor Variables

The factors influencing forest fire spread are divided into four categories: meteorological, terrain, combustible and human factors. The researchers took these four factors into consideration and used statistical inference or machine learning methods to predict the risk of forest fire [42,43]. In forests, the degree of fuel burning is closely related to meteorological factors. Temperature, humidity, precipitation, and wind factors affect the speed at which combustibles reach the ignition point, the direction of combustion, and the spread of combustibles, and, thus, directly affect the spread of forest fires [44]. Therefore, this study collected the hourly temperature, relative humidity, precipitation, wind direction, and wind speed values from the China Meteorological Data Network at the time of the spread of the forest fire.

In terms of terrain factors, altitude and slope can affect the moisture loss of combustibles. In contrast, the aspect affects the amount of solar radiation received by combustibles, directly affecting the combustibles' drying degree. For forests, terrain differences lead to differences in wind, water balance, and heat transfer between different areas, affecting the spread of fire [45]. Therefore, this study obtained the study area's digital elevation model (DEM) data from the Geospatial Data Cloud and extracted the study area's elevation, slope and aspect factors. The type of combustibles is an important factor that directly affects forest fires' spread time and severity [46]. Therefore, this study obtained the combustible type variables of the study area from the Institute of Botany, the Chinese Academy of Sciences. In addition, human factors, such as roads, residential areas, and other surface structures, may block or alter the spread of fire, causing changes in the location of the fire and affecting the direction of the fire spread [47,48]. Therefore, this study downloaded the basic geographic database of the study area from the National Catalogue Service for Geographic Information to collect information on whether there were roads, railways,

residential areas, and water. To summarize, thirteen factors were collected to analyze their impact on forest fires. The specific factors are listed in Table 2.

Table 2. Variables affecting forest fires.

Variable Type	Variable Name	Code	Source
Meteorological	Hourly temperature Relative humidity per hour Precipitation per hour Hourly wind direction Wind speed per hour	Temperature Humidity Precipitation Wind direction Wind speed	China Meteorological Data Network data.cma.cn/ (accessed on 12 February 2022)
Terrain	Elevation Slope Aspect	Elevation Slope Aspect	Geospatial Data Cloud www.gscloud.cn/ (accessed on 14 February 2022)
Combustible	Types of combustibles	Combustible	Institute of Botany, Chinese Academy of Sciences www.ibcas.ac.cn/ (accessed on 18 February 2022)
Human	Road Residential area Railway Water	Road Resa Rail Water	National Catalogue Service for Geographic Information www.webmap.cn/ (accessed on 25 February 2022)

2.4. Extraction of Fire Line and Classification of Fire Severity

Fire intensity refers to the impact or degree of damage of the forest fire on the forest ecosystem [49]. Quantitative evaluation of forest fire intensity is helpful to reveal the development and change of various ecological processes in the ecosystem and the formation mechanism of the forest landscape pattern under the disturbance of forest fire and to analyze the change of regular vegetation coverage and the assessment of vegetation restoration after fire [50,51]. Therefore, it is very important for fire intensity classification. The normalized burn ratio (*NBR*) [52] and the differenced normalized burn ratio (*dNBR*) [53,54] were used to extract the location of the line of fire and the fire state in the remote sensing images. *NBR* is used to identify forest fire burned areas in remote sensing images (Formula (3)). The theoretical value of the *NBR* index ranges from −1 to 1, negatively correlated with forest fire intensity. The *dNBR* threshold method is used to detect the fire state (Formula (4)). The *dNBR* values range from −2 to 2. To facilitate subsequent analysis and processing steps, 1000 was used as a multiplier in the *dNBR* calculation to convert to an integer. Previous studies have used the *dNBR* threshold to extract forest fire intensity levels and have achieved good results. This study selected the threshold range according to previous studies [55–57] and Table 3 shows the threshold range.

$$NBR = \frac{\rho_{nir} - \rho_{swir}}{\rho_{nir} + \rho_{swir}} \quad (3)$$

$$dNBR = NBR_{pre-fire} - NBR_{post-fire} \quad (4)$$

where ρ_{nir} denotes the near-infrared band, ρ_{swir} denotes the short-wave infrared band, $NBR_{pre-fire}$ represents the *NBR* value of the image before the fire, $NBR_{post-fire}$ represents the *NBR* value of the image after the fire.

Table 3. Threshold range for forest fire status.

Fire Severity	1000 × *dNBR* Ranges
Unburned	<299
Low	300–499
Moderate	500–799
High	>800

2.5. Variable Importance Analysis

A random forest method was used to rank the importance of the collected factors and analyze the key factors affecting the spread of the two selected forest fires in Sichuan province. The dependent variable in this study was the occurrence of fire in the grid. A forest fire occurring in a grid was recorded as "1" and no forest fire occurring in a grid as "0". This method directly measured each feature's influence on the model's prediction accuracy. The basic idea is to rearrange the order of eigenvalues in a column and observe how much the model accuracy is reduced [58,59]. This method has little influence on the model accuracy for unimportant features, but it significantly reduces the model accuracy for important features. At the same time, the grid search method was used to specify the model parameter values, and the parameters of the estimated function were optimized through cross-validation to obtain the optimal value. The hyperparameters used by the random forest algorithm are shown in Table 4.

Table 4. Hyperparameter setting of random forest algorithm.

Hyperparameter Name	Value
learning_rate	0.05
n_estimators	1000
max_depth	10
num_leaves	30
min_samples_leaf	1
colsample_bytree	1

The "*Random Forest*" package in R software was used to calculate and rank the importance of each variable. The specific calculation method of the importance of a particular feature X in the random forest was as follows:

(1) for each decision tree in the random forest, the corresponding out-of-bag data (OOB) was used to calculate its out-of-bag data error, denoted as *errOOB*1;
(2) noise interference was randomly added to feature X in all samples of out-of-bag data (so that the value of samples at feature X can be randomly changed), and its out-of-bag data error calculated again, denoted as *errOOB*2.

If there were N variables in the random forest, the feature X importance equation was:

$$Importance = \frac{1}{N}\sum(errOOB2 - errOOB1) \quad (5)$$

2.6. Vegetation Fractional Coverage

Vegetation fractional coverage (*VFC*) is an important indicator reflecting ecological environment monitoring [60]. *VFC* values are between 0 and 1. The closer the value is to 1, the higher the *VFC* of the study area. The value is generally calculated based on the normalized differenced vegetation index (*NDVI*) [61] by a dimidiate pixel model. The calculation method of vegetation coverage was as follows:

$$NDVI = (NIR - R)/(NIR + R) \quad (6)$$

$$VFC = (NDVI - NDVI_{soil})/(NDVI_{veg} - NDVI_{soil}) \quad (7)$$

where *NIR* denotes the near-infrared band, *R* denotes the red band, *VFC* is the vegetation coverage, $NDVI_{soil}$ represents the *NDVI* value of the area with completely bare soil or no vegetation coverage, and $NDVI_{veg}$ represents the *NDVI* value of the pixel completely covered by vegetation.

3. Results

3.1. Extraction of the Fire Line Results

3.1.1. Fire Line Time Series in Muli County

The time series of fire smoke and fire point distribution was obtained from the GF4 data of the Muli County fire (Figure 3). At 11:47 a.m. on 31 March, the fire point was found (Figure 3a). At 13:38 p.m., the region covered by the fire smoke increased significantly (Figure 3b), decreasing at 15:00 p.m. (Figure 3d). However, at 11:52 a.m. on 1 April, the area of smoke from the fire showed an upward trend (Figure 3e), indicating that the fire was intensifying again. As shown in Figure 3, there was a lot of thick smoke at the fire scene, and the fire spread to the north–northeast, consistent with the local weather conditions.

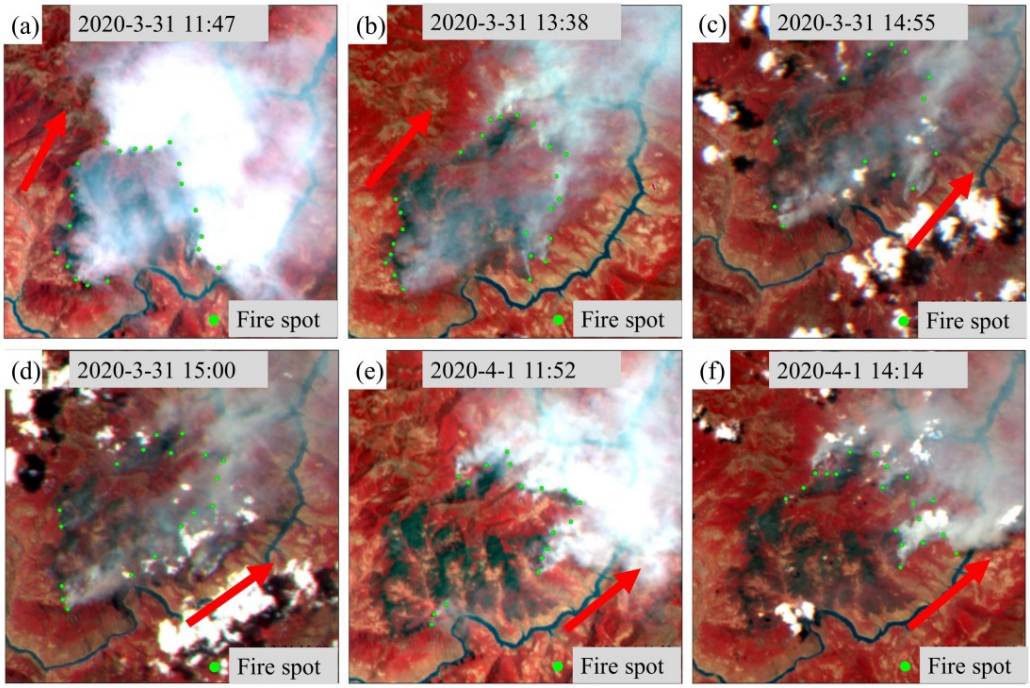

Figure 3. Forest fire monitoring in Muli County based on GF-4 satellite data. (**a**–**f**) are the fire and smoke distribution at 11:47 a.m. on 31 March, 13:38 p.m. on 31 March, 14:55 p.m. on 31 March, 15:00 p.m. on 31 March, 11:52 a.m. on 1 April and 14:14 p.m. on 1 April in 2020, respectively.

The location and shape of the fire line were extracted from multi-source remote sensing data (Figure 4). At 12:45 p.m. on 29 March, the image monitoring indicated that the burned area was 1.05 km^2 (Figure 4a). At 11:45 a.m. on 30 March, the burned area was 8.97 km^2 (Figure 4b), and by 12:30 p.m., the burned area had reached 17.08 km^2 (Figure 4d), within 45 min, and the fire spread by 8.11 km^2. By 14:05 p.m. on 31 March, the fire burned area reached 106.35 km^2 (Figure 4f). The rapid spread of this stage brought great difficulties to the rescue. By 11:35 a.m. on 1 April, the fire burned area was 125.89 km^2 (Figure 4g), and the fire was initially controlled at this timepoint. However, the fire reignited again, due to the sudden change of wind direction and the accelerated wind speed. On 5 April, the fire was controlled and extinguished, and the final burnt area was 209.17 km^2 (Figure 4i).

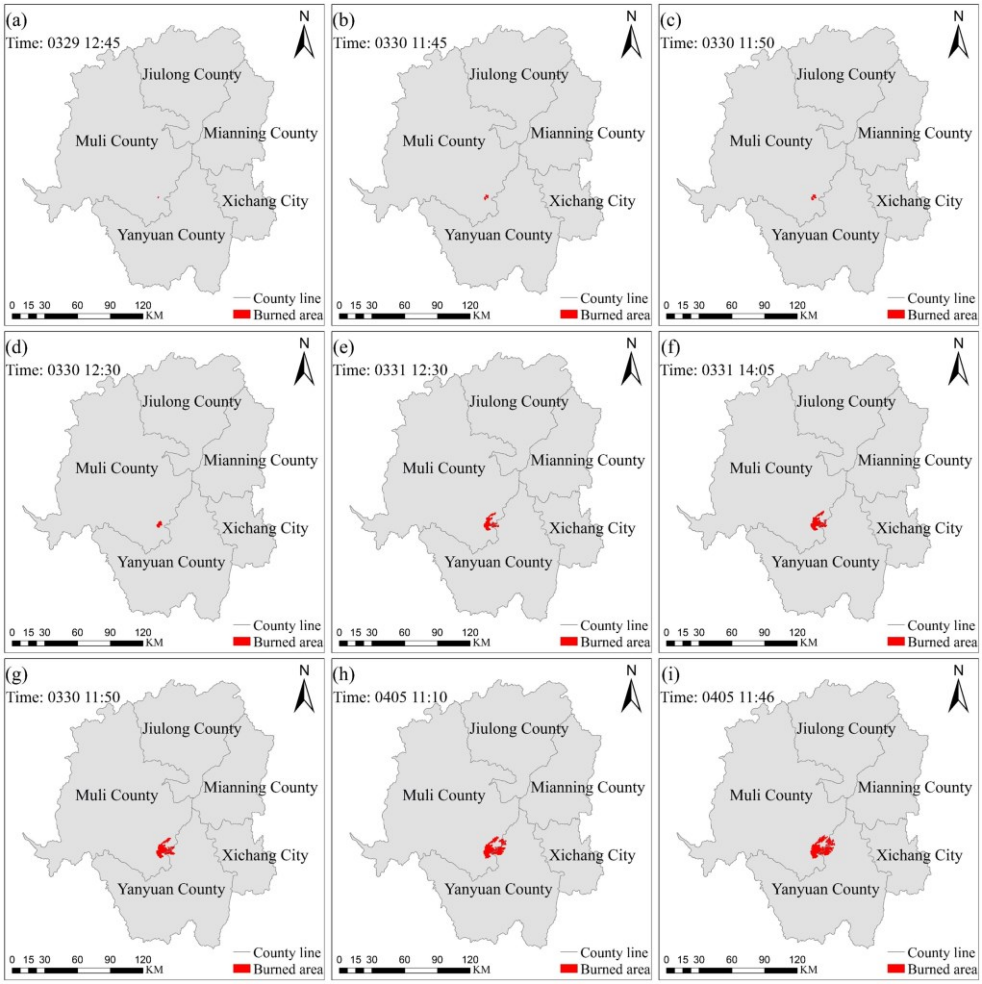

Figure 4. Multi-source satellite remote sensing image extraction of the burned area in Muli County. (**a**) at 12:45 p.m. on 29 March, (**b**) at 11:45 a.m. on 30 March, (**c**) at 11:50 a.m. on 30 March, (**d**) at 12:30 p.m. on 30 March, (**e**) at 12:30 p.m. on 31 March, (**f**) at 14:05 p.m. on 31 March, (**g**) at 11:35 a.m. on 1 April, (**h**) at 11:10 a.m. on 5 April, (**i**) at 11:46 a.m. on 5 April in 2020.

3.1.2. Fire Line Time Series in Jingjiu Township

The fire smoke and fire point distribution time series were obtained by GF-4 data of the Jingjiu Township (Figure 5). At 11:47 a.m. on 31 March, the fire point was found in Jingjiu Township (Figure 5a). At 14:55 p.m., the fire smoke decreased (Figure 5b), while later, at 16:41 p.m., the area covered by fire smoke increased significantly (Figure 5c). However, by 11:52 a.m. on 1 April, the region of the fire smoke showed a downward trend again (Figure 5d). By 15:17 p.m. on 1 April, only a small amount of smoke and sporadic fire spots was observed at the scene, showing that the fire had been brought under effective control (Figure 5f). According to the trend analysis in the figure, the fire gradually moved to the east–northeast, consistent with the local weather conditions. This supports the important application value of the GF-4 satellite multispectral data in fire spread monitoring.

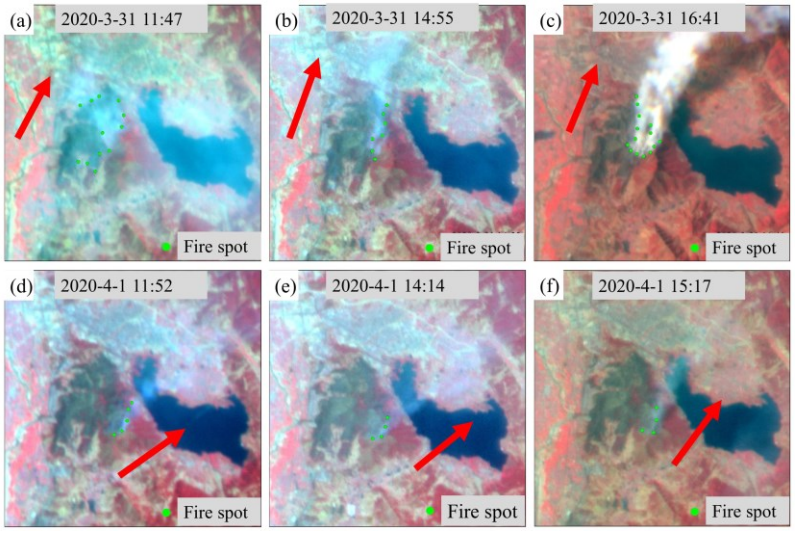

Figure 5. Forest fire monitoring in Jingjiu Township based on GF-4 satellite data. (**a**–**f**) are the fire and smoke distribution at 11:47 a.m. on 31 March, 14:55 p.m. on 31 March, 16:41 p.m. on 31 March, 11:52 a.m. on 1 April, 14:14 p.m. on 1 April and 15:17 p.m. on 1 April in 2020, respectively.

The fire line time series of Jingjiu Township was extracted from multi-source remote sensing data (Figure 6). At 13:20 p.m. on 30 March, the burned area was 2.80 km^2 (Figure 6a), and by 10:55 a.m. on 31 March, the burned area had reached 12.10 km^2 (Figure 6b). By 14:55 p.m., the fire burned area had risen up to 17.98 km^2 (Figure 6d), and the fire at this stage had an accelerating trend. By 15:17 p.m. on 1 April, the fire burned area had reached 26.45 km^2 (Figure 6h), and the fire was under control at this time. The fire was extinguished on 2 April, and the final area burned was 30.91 km^2.

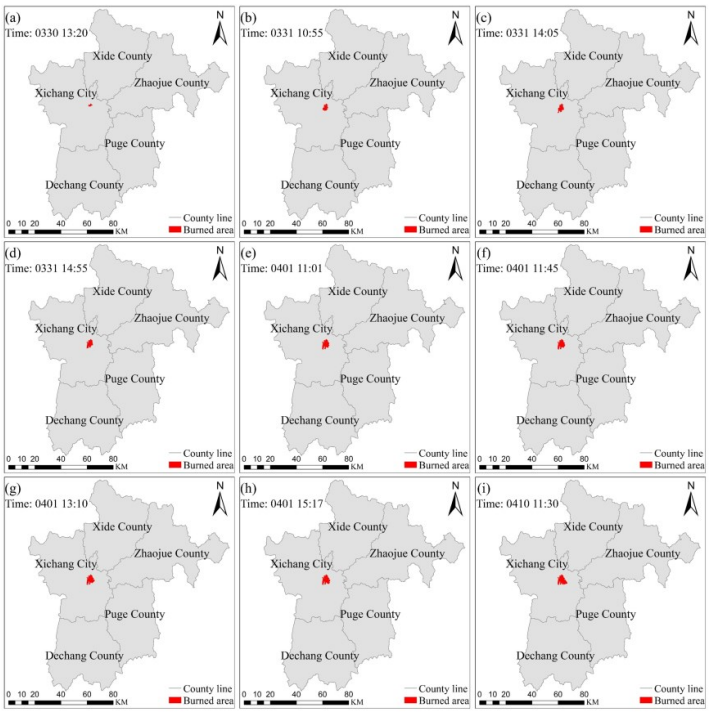

Figure 6. Multi-source satellite remote sensing image extraction of the burned area in Jingjiu Township. (**a**) at 13:20 p.m. on 30 March, (**b**) at 10:55 a.m. on 31 March, (**c**) at 14:05 p.m. on 31 March, (**d**) at 14:55 p.m. on 31 March, (**e**) at 11:01 a.m. on 1 April, (**f**) at 11:45 a.m. on 1 April, (**g**) at 13:10 p.m. on 1 April, (**h**) at 15:17 p.m. on 1 April, (**i**) at 11:30 a.m. on 10 April in 2020.

3.2. Extraction of Forest Fire Intensity Results

The final fire burned area in Muli County was 209.17 km^2. The final fire burned area was classified according to the dNBR threshold (Figure 7a). The low-intensity burned area was 138.66 km^2, accounting for 66.29%, the moderate-intensity burned area was 36.51 km^2, accounting for 17.45%, and the high-intensity burned area was 34.00 km^2, accounting for 16.26%. The final burned area of the Jingjiu Township was 30.91 km^2. The forest fire intensity classification in the final burned area was performed according to the dNBR threshold (Figure 7b). The low-intensity burned area was 23.70 km^2, accounting for 76.67%, the moderate-intensity burned area was 5.51 km^2, accounting for 17.83%, and the high-intensity burned area was 1.70 km^2, 5.50% of the total area.

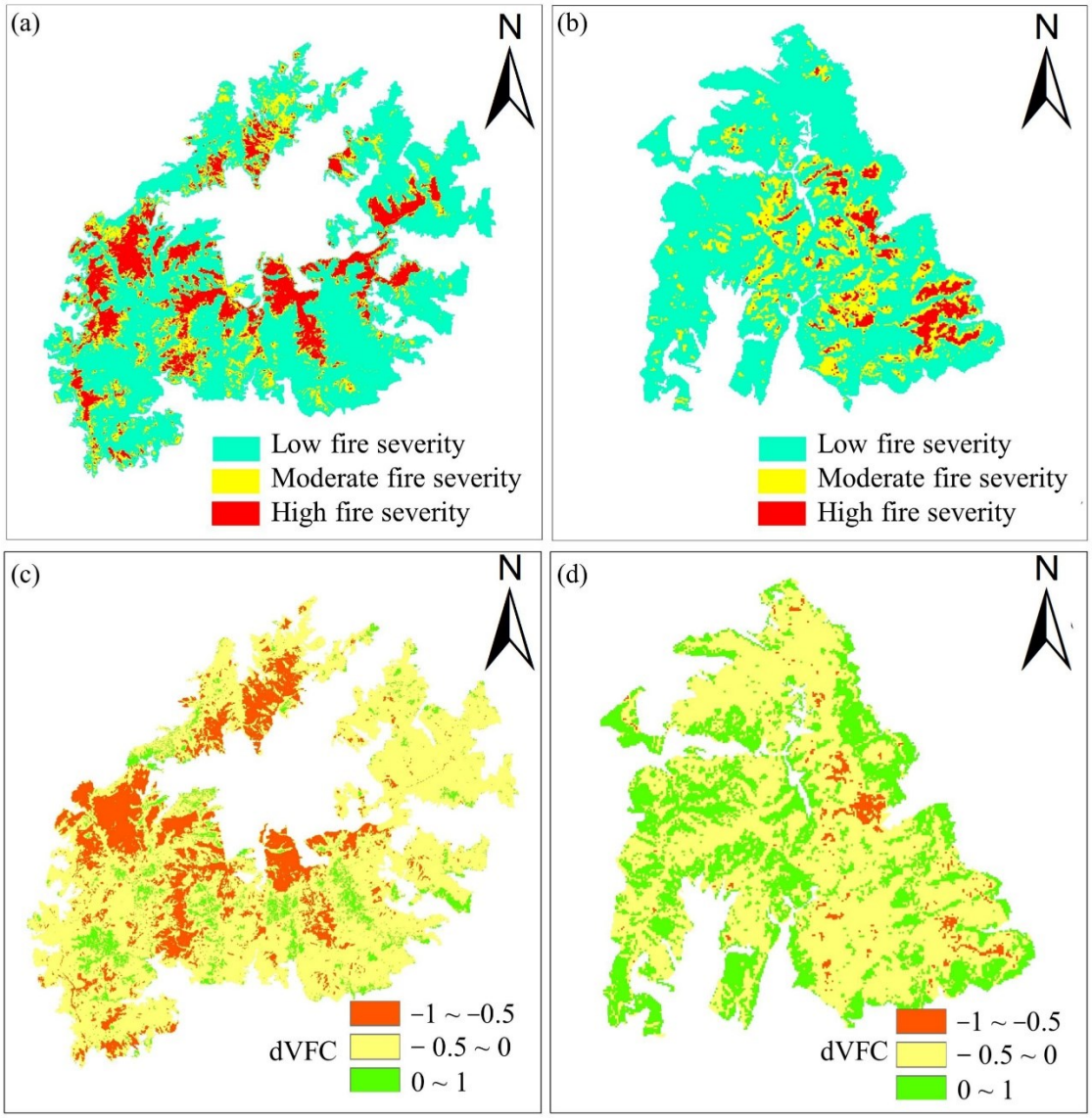

Figure 7. Fire intensity and the difference between the post-fire *VFC* and the pre-fire *VFC* (d*VFC*) distributions in Muli County and Jingjiu Township. (**a**,**b**) fire intensity distributions in Mulli County and Jingjiu Township, respectively. (**c**,**d**) the d*VFC* distributions in Mulli County and Jingjiu Township, respectively.

3.3. Variable Importance

A random forest algorithm was used to rank 13 variables of forest fire spread (Figure 8). The relative humidity was the most important variable affecting the spreads of the two

selected forest fires in Sichuan Province, followed by temperature. Altitude had the greatest impact among terrain factors, while other terrain factors (slope, aspect) had relatively weak effects on the forest fire spread. The importance of combustible type was higher, below only relative humidity and temperature. The importance of human factors was overall lower, while the location in residential areas and rivers was higher than roads and railways.

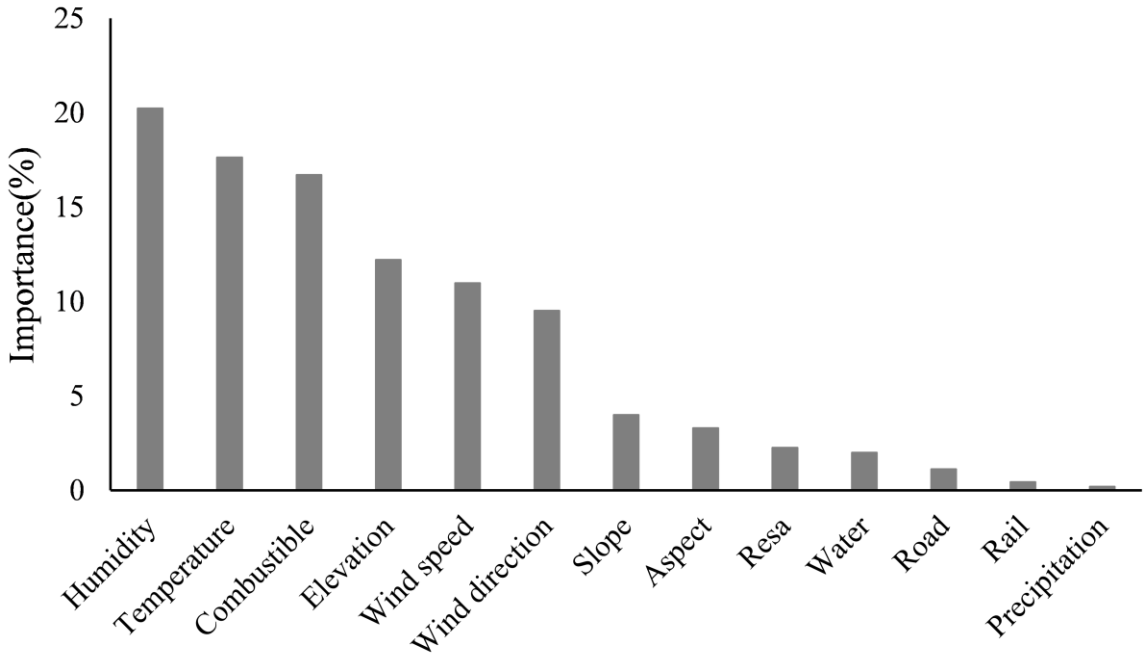

Figure 8. The random forest algorithm ranking of the importance of the 13 analyzed variables.

3.4. Changes in Vegetation Coverage

The vegetation coverage of Muli County is depicted before the fire and one year after the fire (Figure 9a,b) and Jingjiu Township before and one year after the fire (Figure 9c,d), respectively. In this study, 40 points were randomly selected from the pre-fire *VFC*, the post-fire *VFC* and the dNBR images, respectively, to build the relationship between the *VFC* and dNBR, respectively (Figure 10). The results for Muli County and Jingjiu Township were similar. Both pre-fire *VFC*s were significantly proportional to dNBR, with an R^2 of 0.79 and 0.76, respectively (Figure 10a,c). Both post-fire *VFC*s were inversely proportional to dNBR, with an R^2 of 0.77 and 0.74, respectively (Figure 10b,d).

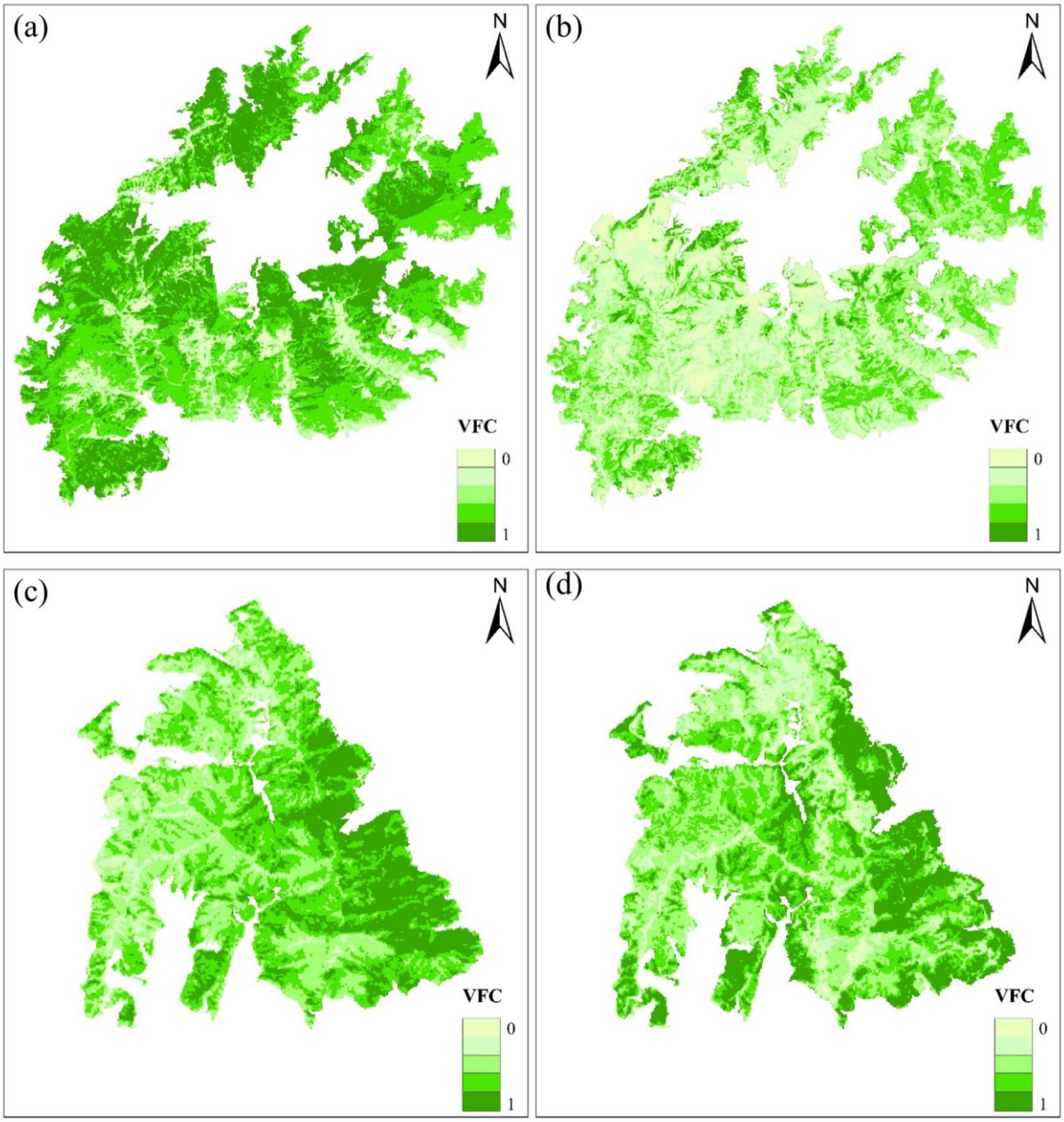

Figure 9. Changes in vegetation coverage before and after the fire. (**a**,**b**) the *VFC* before and after the fire in Muli County, respectively, (**c**,**d**) the *VFC* before and after the fire in Jingjiu Township, respectively.

The difference between the post-fire *VFC* and the pre-fire *VFC* (d*VFC*) (Figure 7c,d), indicated that the *VFC* recovery effect of different degrees of fire was significantly different. The *VFC* in the low-intensity burned area could be restored to its original state. After a long time of natural recovery, the *VFC* in the moderate-intensity burned area still had a certain gap from the original *VFC*. However, even after a long time of recovery, the *VFC* was still far from the original in the high-intensity burned area.

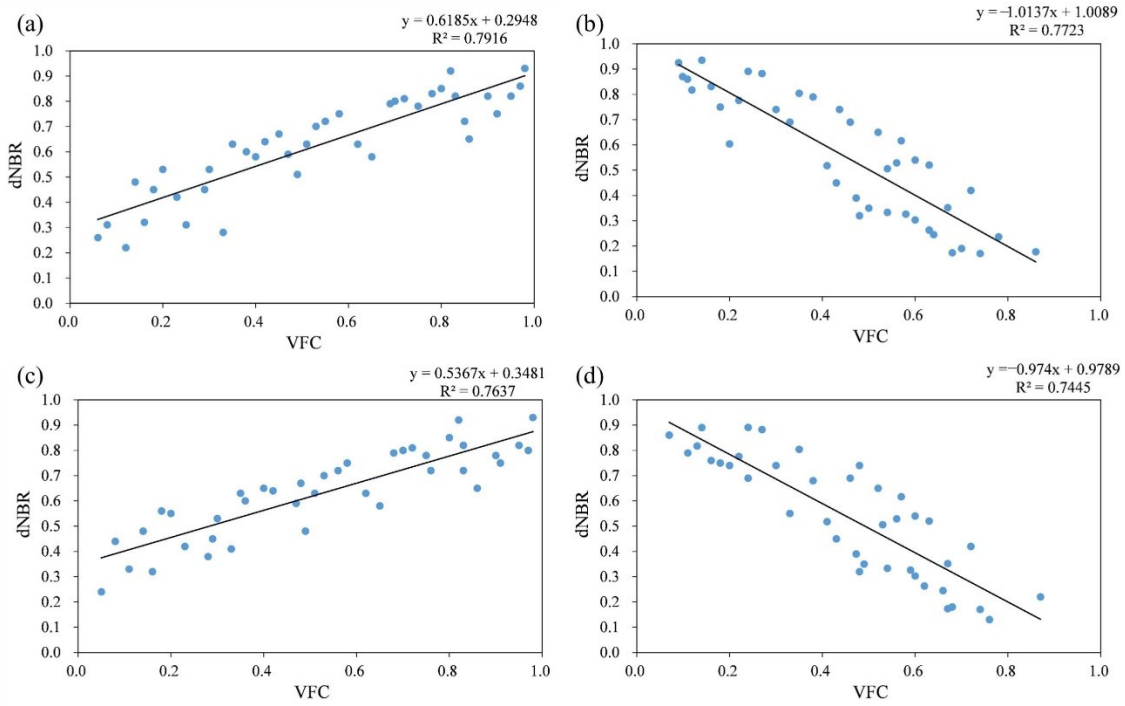

Figure 10. The relationship between vegetation coverage before and after fire, and dNBR. (**a**,**b**) the fitting curves of *VFC* before and after the fire, and dNBR in Muli County, respectively, (**c**,**d**) the fitting curves of *VFC* before and after the fire, and dNBR in Jingjiu Township, respectively.

4. Discussion

With frequent forest fires and massive losses, it is crucial to use remote sensing to understand and monitor the spread of forest fires [62,63]. By acquiring multi-source remote sensing data to extract the process of spreading of a forest fire, great value is added to analyzing the development of a regular fire time series. In this study, 29 remote sensing images were obtained from two forest fires in Sichuan Province, and the burned areas were extracted in time series. In terms of forest fire monitoring, comprehensive multi-source remote sensing images have the advantages of being low cost, accurate and efficient. They play an important role in fire spot identification and burned area extraction.

Due to low resolution and low accuracy, the medium- and low-resolution satellite remote sensing images are only suitable for monitoring large-scale forest fires. With such images, it is difficult to timely and accurately obtain fire location information for small area forest fires [64]. The emergence of a new generation of remote sensing satellites has made up for the lack of spatial and temporal resolution of traditional remote sensing information. It has become an essential supplement to satellite forest fire monitoring services. High spatial resolution can provide more detailed and accurate forest fire information, such as smoke and fire conditions [65]. However, the large storage space and low data processing efficiency, due to high spatial resolution, mean its wide range of industrial applications can be limited. To accurately grasp the information and dynamics of forest fires, efficient and reliable forest fire recognition algorithms are particularly important. Here, this study used the normalized burned ratio (NBR) and the difference normalized burned ratio (dNBR) of multiple phase differences to extract the fire line and forest fire status. The NBR index represents an improvement on the normalized difference vegetation index (NDVI), and dNBR, which uses a multi-temporal approach, when combined with the NBR index, can more accurately extract fire lines and define fire situations. Its increased accuracy was similarly observed in previous research [66]. Therefore, combining the advantages of multi-source satellite remote sensing data can effectively display forest fire information and monitor the spread and development of forest fires.

The hourly relative humidity, temperature, precipitation, wind speed and wind direction were selected as the five important meteorological factors affecting the spread of the two selected forest fires in Sichuan Province. Meteorological factors have a more significant impact on fire spread than other factors. The variable importance results showed that relative humidity was the most critical factor affecting the spread of forest fires in the study area. The temperature was second only to relative humidity, and wind speed and direction were more important than precipitation. Relative humidity affects the fire fuel moisture contents in forests, and high relative humidity increases fuel moisture, thereby slowing the fire spread. Temperature directly affects the moisture content of combustible fuels. High temperatures can increase plant transpiration and lower the moisture content of potential fire fuels, therefore increasing the likelihood of forest fire spread. Increased wind speed and direction can accelerate forest moisture loss and expand fire spread [67–69]. In March 2020, the southwest region suffered from drought and little rain, with temperatures significantly higher than in previous years and more windy weather. Moreover, there was no rain for 20 consecutive days with less than 10% humidity. Extreme weather conditions have significantly increased the likelihood of forest fires starting and spreading in the study area. It is worth noting that although temperature was an important variable among the meteorological factors affecting fire spread in this study, previous studies have shown that high temperature appears to inhibit the occurrence and spread of fires in Fujian [70]. Previous research suggests a threshold between temperature and forest fires [71]. It is also possible that forest managers' increased awareness of fire prevention has dramatically reduced the spread of fires during periods of high temperature, as supported by relevant researchers [72]. Among terrain factors, altitude was the most crucial factor affecting the spread of forest fires in the study area. An increase in altitude slows the fire spread to some extent. Due to the particularity of the low-pressure and low-oxygen environment at high altitudes, insufficient oxygen reduces the speed of fire spread. The terrain aspect was less important than elevation. This may be because, in the study's area terrain, the solar radiation differences caused by variations in the aspect were not very different, resulting in the terrain aspect having a small impact [73,74]. The type of combustible is an indicator that directly determines whether the forest is combustible, and directly affects the process of fire spreading [26,39]. Therefore, its importance was higher, second only to relative humidity and temperature. It has been shown that the spread of forest fires can be related to human activities and surface structures [75,76]. Therefore, this study collected data on the presence or absence of railways, roads, residential areas, and water in the fires analyzed. Surface structures, such as roads and water, belonging to human factors, have a blocking effect on the spread of forest fires to a certain extent. Due to human factors, the spread of forest fires may slow down, or the direction of the spread might change. Moreover, due to artificial surface structures, the population density and the degree of population aggregation could affect the spread process [77]. However, the results showed that these land cover type variables were of relatively low importance compared to other variables, similar to the results of previous studies [78,79]. This may be related to the low population density in the study area, with most of the population concentrated in areas with developed industries and low forest coverage. However, due to the uncontrollable characteristics of human factors, further attention should be given to such factors in managing and preventing forest fires in the future.

The vegetation coverage before and after fire in the study area was calculated, and the relationship between vegetation coverage and dNBR was explored. The pre-fire *VFC* was obviously proportional to the dNBR, and the post-fire *VFC* was inversely proportional to the dNBR. This indicates that the lower the vegetation coverage, the lower the fire severity, and vice versa. Moreover, the higher the fire severity, the poorer the vegetation recovery ability is after the fire. *VFC* recovery effects differed in different degrees of burned areas based on d*VFC* distribution (Figure 7c,d). The *VFC* in the low-intensity burned area could return to its original state after a certain period of time, and might even exceed the pre-fire *VFC*. This is because low-intensity fires can have a certain vegetation promoting effect on

forests [80,81]. In the burned area with moderate intensity, there was still a certain gap between the original *VFC* and the natural recovery after a long period of time. However, in the high-intensity burned area, even after a long time of recovery, there was still a large difference compared to the original *VFC*. This is because moderate-intensity and high-intensity fires destroy the forest structure, making it difficult for the forest to recover quickly [82,83]. Therefore, it is imperative to reduce forest fire occurrence and monitor the spread and development of fire in time to protect forest resources.

At present, a single source of remote sensing data cannot simultaneously meet the temporal resolution and spatial resolution requirements of fire spread monitoring, which affects its efficiency and timeliness [84]. To solve this problem, this study collected multi-source image data widely used in forest fire monitoring to improve forest fire spread monitoring. Many studies have used remote sensing data for forest fire spread monitoring [35–39]. Such approaches have the advantages of a wide monitoring range and high precision. However, monitoring the development and spread of small and short-duration forest fires is still difficult. How to fully combine multi-source remote sensing data to give full play to the advantages of various types of forest fire spread monitoring is an urgent problem to be solved. The lack of forest fire spread monitoring may directly lead to the inability to comprehensively analyze the process and regular characteristics of forest fire spread, resulting in delays and errors in the judgment and management of forest fires.

5. Conclusions

In this study, the forest fires in Muli County and Jingjiu Township, Sichuan Province, were monitored with multiple satellite remote sensing image data, and the importance of forest fire factors was investigated and quantified. In addition, the dNBR was used to identify the burned area and forest fire intensity. The relationship between the vegetation coverage before and after the fire and forest fire intensity was analyzed. The results show that by combining the remote sensing data obtained by multi-source satellite remote sensing, the monitoring and quantitative analysis of the dynamic spread of wildfires can be carried out. This enables an accurate and macroscopic analysis of regular fire spread. For the forest fires in Sichuan Province studied here, meteorological factors had the most significant impact on their spread compared with other forest fire factors. Among all variables, relative humidity was the most important factor affecting forest fire spread, followed by temperature. The linear regression results showed that *VFC* before and after fire and dNBR were significantly correlated, and *VFC* recovery varied according to fire severity. Such results can also be used to supplement the rescue efforts of forest firefighters. In this study, only the forest fire spread data of Sichuan Province were collected, and the results obtained are only applicable to the study area, but still have important reference value for other regions. In the future, forest fire data from other places will also be collected to further develop a comprehensive understanding of forest fires across the country. To conclude, the results of this study not only provide information about the fires in Sichuan Province, they can also be implemented as a technical reference for wildfire remote sensing spread monitoring and emergency response.

Author Contributions: Conceptualization, M.L. and B.W.; methodology, Y.T.; software, Z.W.; validation, M.L. and B.W.; formal analysis, X.Z.; investigation, Z.W.; resources, M.L.; data curation, M.L.; writing—original draft preparation, Y.T.; writing—review and editing, Z.W.; visualization, X.Z.; supervision, Y.T.; project administration, B.W.; funding acquisition, M.L. All authors have read and agreed to the published version of the manuscript.

Funding: This research was funded by University of Science and Technology of China and the Fundamental Research Funds for the Central Universities. The grant numbers are 2020YFC1511603 and 2572020BA07 respectively.

Data Availability Statement: The data used in the study are available from the authors and can be shared upon reasonable requests.

Conflicts of Interest: The authors declare no conflict of interest.

References

1. Li, Q.; Cui, J.; Jiang, W.; Jiao, Q.; Gong, L.; Zhang, J.; Shen, X. Monitoring of the Fire in Muli County on March 28, 2020, based on high temporal-spatial resolution remote sensing techniques. *Nat. Hazards Res.* **2021**, *1*, 20–31. [CrossRef]
2. Van Leeuwen, W.J.; Casady, G.M.; Neary, D.G.; Bautista, S.; Alloza, J.A.; Carmel, Y.; Wittenberg, L.; Malkinson, D.; Orr, B.J. Monitoring post-wildfire vegetation response with remotely sensed time-series data in Spain, USA and Israel. *Int. J. Wildland Fire* **2010**, *19*, 75–93. [CrossRef]
3. Van Leeuwen, W.J. Monitoring the effects of forest restoration treatments on post-fire vegetation recovery with MODIS multitemporal data. *Sensors* **2008**, *8*, 2017–2042. [CrossRef]
4. Islam, S.; Bhuiyan, M.A.H. Sundarbans mangrove forest of Bangladesh: Causes of degradation and sustainable management options. *Environ. Sustain.* **2018**, *1*, 113–131. [CrossRef]
5. Khan, A.; Gupta, S.; Gupta, S.K. Multi-hazard disaster studies: Monitoring, detection, recovery, and management, based on emerging technologies and optimal techniques. *Int. J. Disaster Risk Reduct.* **2020**, *47*, 101642. [CrossRef]
6. Kulakowski, D.; Seidl, R.; Holeksa, J.; Kuuluvainen, T.; Nagel, T.A.; Panayotov, M.; Svoboda, M.; Thorn, S.; Vacchiano, G.; Whitlock, C. A walk on the wild side: Disturbance dynamics and the conservation and management of European mountain forest ecosystems. *For. Ecol. Manag.* **2017**, *388*, 120–131. [CrossRef]
7. Wu, Z.; Li, M.; Wang, B.; Quan, Y.; Liu, J. Using artificial intelligence to estimate the probability of forest fires in Heilongjiang, northeast China. *Remote Sens.* **2021**, *13*, 1813. [CrossRef]
8. Pham, B.T.; Jaafari, A.; Avand, M.; Al-Ansari, N.; Dinh Du, T.; Yen, H.P.H.; Phong, T.V.; Nguyen, D.H.; Le, H.V.; Mafi-Gholami, D. Performance evaluation of machine learning methods for forest fire modeling and prediction. *Symmetry* **2020**, *12*, 1022. [CrossRef]
9. Matin, M.A.; Chitale, V.S.; Murthy, M.S.; Uddin, K.; Bajracharya, B.; Pradhan, S. Understanding forest fire patterns and risk in Nepal using remote sensing, geographic information system and historical fire data. *Int. J. Wildland Fire* **2017**, *26*, 276–286. [CrossRef]
10. Montealegre, A.L.; Lamelas, M.T.; Tanase, M.A.; De la Riva, J. Forest fire severity assessment using ALS data in a Mediterranean environment. *Remote Sens.* **2014**, *6*, 4240–4265. [CrossRef]
11. Gibson, R.; Danaher, T.; Hehir, W.; Collins, L. A remote sensing approach to mapping fire severity in south-eastern Australia using sentinel 2 and random forest. *Remote Sens. Environ.* **2020**, *240*, 111702. [CrossRef]
12. NorTh, M.P.; STePhens, S.L.; Collins, B.M.; Agee, J.K.; APleT, G.; FrAnklin, J.F.; Fulé, P.Z. Reform forest fire management. *Science* **2015**, *349*, 1280–1281. [CrossRef] [PubMed]
13. Allison, R.S.; Johnston, J.M.; Craig, G.; Jennings, S. Airborne optical and thermal remote sensing for wildfire detection and monitoring. *Sensors* **2016**, *16*, 1310. [CrossRef]
14. Yuan, C.; Liu, Z.; Zhang, Y. Fire detection using infrared images for UAV-based forest fire surveillance. In Proceedings of the 2017 International Conference on Unmanned Aircraft Systems (ICUAS), Miami, FL, USA, 13–16 June 2017; pp. 567–572.
15. Sudhakar, S.; Vijayakumar, V.; Kumar, C.S.; Priya, V.; Ravi, L.; Subramaniyaswamy, V. Unmanned Aerial Vehicle (UAV) based Forest Fire Detection and monitoring for reducing false alarms in forest-fires. *Comput. Commun.* **2020**, *149*, 1–16. [CrossRef]
16. Quintano, C.; Fernández-Manso, A.; Stein, A.; Bijker, W. Estimation of area burned by forest fires in Mediterranean countries: A remote sensing data mining perspective. *For. Ecol. Manag.* **2011**, *262*, 1597–1607. [CrossRef]
17. Roy, D.P.; Wulder, M.A.; Loveland, T.R.; Woodcock, C.E.; Allen, R.G.; Anderson, M.C.; Helder, D.; Irons, J.R.; Johnson, D.M.; Kennedy, R. Landsat-8: Science and product vision for terrestrial global change research. *Remote Sens. Environ.* **2014**, *145*, 154–172. [CrossRef]
18. Bisquert, M.; Caselles, E.; Sánchez, J.M.; Caselles, V. Application of artificial neural networks and logistic regression to the prediction of forest fire danger in Galicia using MODIS data. *Int. J. Wildland Fire* **2012**, *21*, 1025–1029. [CrossRef]
19. Justice, C.; Townshend, J.; Vermote, E.; Masuoka, E.; Wolfe, R.; Saleous, N.; Roy, D.; Morisette, J. An overview of MODIS Land data processing and product status. *Remote Sens. Environ.* **2002**, *83*, 3–15. [CrossRef]
20. Drusch, M.; Del Bello, U.; Carlier, S.; Colin, O.; Fernandez, V.; Gascon, F.; Hoersch, B.; Isola, C.; Laberinti, P.; Martimort, P. Sentinel-2: ESA's optical high-resolution mission for GMES operational services. *Remote Sens. Environ.* **2012**, *120*, 25–36. [CrossRef]
21. Yang, A.; Zhong, B.; Wu, S.; Liu, Q. Radiometric cross-calibration of GF-4 in multispectral bands. *Remote Sens.* **2017**, *9*, 232. [CrossRef]
22. Jia, K.; Liang, S.; Gu, X.; Baret, F.; Wei, X.; Wang, X.; Yao, Y.; Yang, L.; Li, Y. Fractional vegetation cover estimation algorithm for Chinese GF-1 wide field view data. *Remote Sens. Environ.* **2016**, *177*, 184–191. [CrossRef]
23. Helman, D.; Bahat, I.; Netzer, Y.; Ben-Gal, A.; Alchanatis, V.; Peeters, A.; Cohen, Y. Using time series of high-resolution planet satellite images to monitor grapevine stem water potential in commercial vineyards. *Remote Sens.* **2018**, *10*, 1615. [CrossRef]
24. Wulder, M.; White, J.; Alvarez, F.; Han, T.; Rogan, J.; Hawkes, B. Characterizing boreal forest wildfire with multi-temporal Landsat and LIDAR data. *Remote Sens. Environ.* **2009**, *113*, 1540–1555. [CrossRef]
25. Yuan, C.; Liu, Z.; Zhang, Y. Aerial images-based forest fire detection for firefighting using optical remote sensing techniques and unmanned aerial vehicles. *J. Intell. Robot. Syst.* **2017**, *88*, 635–654. [CrossRef]
26. Hua, L.; Shao, G. The progress of operational forest fire monitoring with infrared remote sensing. *J. For. Res.* **2017**, *28*, 215–229. [CrossRef]
27. Tao, G.; Jia, K.; Zhao, X.; Wei, X.; Xie, X.; Zhang, X.; Wang, B.; Yao, Y.; Zhang, X. Generating high spatio-temporal resolution fractional vegetation cover by fusing GF-1 WFV and MODIS data. *Remote Sens.* **2019**, *11*, 2324. [CrossRef]

28. Chowdhury, E.H.; Hassan, Q.K. Operational perspective of remote sensing-based forest fire danger forecasting systems. *ISPRS J. Photogramm. Remote Sens.* **2015**, *104*, 224–236. [CrossRef]
29. Wei, X.; Bai, K.; Chang, N.-B.; Gao, W. Multi-source hierarchical data fusion for high-resolution AOD mapping in a forest fire event. *Int. J. Appl. Earth Obs. Geoinf.* **2021**, *102*, 102366. [CrossRef]
30. Coops, N.C.; Tompalski, P.; Goodbody, T.R.; Achim, A.; Mulverhill, C. Framework for near real-time forest inventory using multi source remote sensing data. *For. Int. J. For. Res.* **2022**, *15*, 1–19. [CrossRef]
31. Bolton, D.K.; Coops, N.C.; Hermosilla, T.; Wulder, M.A.; White, J.C. Assessing variability in post-fire forest structure along gradients of productivity in the Canadian boreal using multi-source remote sensing. *J. Biogeogr.* **2017**, *44*, 1294–1305. [CrossRef]
32. Kganyago, M.; Shikwambana, L. Assessment of the characteristics of recent major wildfires in the USA, Australia and Brazil in 2018–2019 using multi-source satellite products. *Remote Sens.* **2020**, *12*, 1803. [CrossRef]
33. Li, X.; Zhang, M.; Zhang, S.; Liu, J.; Sun, S.; Hu, T.; Sun, L. Simulating forest fire spread with cellular automation driven by a LSTM based speed model. *Fire* **2022**, *5*, 13. [CrossRef]
34. Nebot, À.; Mugica, F. Forest Fire Forecasting Using Fuzzy Logic Models. *Forests* **2021**, *12*, 1005. [CrossRef]
35. Wu, X.; Liu, T.; Cheng, Y.; Wang, L.; Guo, Y.; Zhang, Y.; He, J. Dynamic monitoring of straw burned area using multi-source satellite remote sensing data. *Trans. Chin. Soc. Agric. Eng.* **2017**, *33*, 153–159.
36. Xiaofeng, Z.; Xianlin, Q.; Lingyu, Y.; Xiaozhong, C.; Xiangqing, Z. Decision tree method for burned area identification based on the spectral index of GF-1 WFV image. *For. Resour. Wanagement* **2015**, *28*, 73.
37. Flannigan, M.D.; Haar, T.V. Forest fire monitoring using NOAA satellite AVHRR. *Can. J. For. Res.* **1986**, *16*, 975–982. [CrossRef]
38. Kaufman, Y.J.; Justice, C.O.; Flynn, L.P.; Kendall, J.D.; Prins, E.M.; Giglio, L.; Ward, D.E.; Menzel, W.P.; Setzer, A.W. Potential global fire monitoring from EOS-MODIS. *J. Geophys. Res. Atmos.* **1998**, *103*, 32215–32238. [CrossRef]
39. Dwyer, E.; Grégoire, J.-M.; Malingreau, J.-P. A global analysis of vegetation fires using satellite images: Spatial and temporal dynamics. *Ambio* **1998**, *27*, 175–181.
40. Belgiu, M.; Stein, A. Spatiotemporal image fusion in remote sensing. *Remote Sens.* **2019**, *11*, 818. [CrossRef]
41. Viana, C.M.; Girão, I.; Rocha, J. Long-term satellite image time-series for land use/land cover change detection using refined open-source data in a rural region. *Remote Sens.* **2019**, *11*, 1104. [CrossRef]
42. Parisien, M.-A.; Snetsinger, S.; Greenberg, J.A.; Nelson, C.R.; Schoennagel, T.; Dobrowski, S.Z.; Moritz, M.A. Spatial variability in wildfire probability across the western United States. *Int. J. Wildland Fire* **2012**, *21*, 313–327. [CrossRef]
43. Salavati, G.; Saniei, E.; Ghaderpour, E.; Hassan, Q.K. Wildfire risk forecasting using weights of evidence and statistical index models. *Sustainability* **2022**, *14*, 3881. [CrossRef]
44. Seager, R.; Hooks, A.; Williams, A.P.; Cook, B.; Nakamura, J.; Henderson, N. Climatology, variability, and trends in the US vapor pressure deficit, an important fire-related meteorological quantity. *J. Appl. Meteorol. Climatol.* **2015**, *54*, 1121–1141. [CrossRef]
45. Pimont, F.; Dupuy, J.-L.; Linn, R. Coupled slope and wind effects on fire spread with influences of fire size: A numerical study using FIRETEC. *Int. J. Wildland Fire* **2012**, *21*, 828–842. [CrossRef]
46. Clarke, P.J.; Knox, K.J.; Bradstock, R.A.; Munoz-Robles, C.; Kumar, L. Vegetation, terrain and fire history shape the impact of extreme weather on fire severity and ecosystem response. *J. Veg. Sci.* **2014**, *25*, 1033–1044. [CrossRef]
47. Ricotta, C.; Di Vito, S. Modeling the landscape drivers of fire recurrence in Sardinia (Italy). *Environ. Manag.* **2014**, *53*, 1077–1084. [CrossRef]
48. Lein, J.K.; Stump, N.I. Assessing wildfire potential within the wildland–urban interface: A southeastern Ohio example. *Appl. Geogr.* **2009**, *29*, 21–34. [CrossRef]
49. Lentile, L.B.; Smith, F.W.; Shepperd, W.D. Influence of topography and forest structure on patterns of mixed severity fire in ponderosa pine forests of the South Dakota Black Hills, USA. *Int. J. Wildland Fire* **2006**, *15*, 557–566. [CrossRef]
50. Sawyer, R.; Bradstock, R.; Bedward, M.; Morrison, R.J. Fire intensity drives post-fire temporal pattern of soil carbon accumulation in Australian fire-prone forests. *Sci. Total Environ.* **2018**, *610*, 1113–1124. [CrossRef]
51. Halofsky, J.E.; Peterson, D.L.; Harvey, B.J. Changing wildfire, changing forests: The effects of climate change on fire regimes and vegetation in the Pacific Northwest, USA. *Fire Ecol.* **2020**, *16*, 4. [CrossRef]
52. Key, C.H.; Benson, N.C. Landscape assessment: Remote sensing of severity, the normalized burn ratio and ground measure of severity, the composite burn index. In *FIREMON: Fire Effects Monitoring and Inventory System*; USDA Forest Service, Rocky Mountain Res. Station: Ogden, UT, USA, 2005.
53. Epting, J.; Verbyla, D.; Sorbel, B. Evaluation of remotely sensed indices for assessing burn severity in interior Alaska using Landsat TM and ETM+. *Remote Sens. Environ.* **2005**, *96*, 328–339. [CrossRef]
54. Brewer, C.K.; Winne, J.C.; Redmond, R.L. Classifying and mapping wildfire severity: A comparison of methods. *Photogramm. Eng. Remote Sens.* **2005**, *71*, 1311–1320. [CrossRef]
55. Wu, Z.; Wang, B.; Li, M.; Tian, Y.; Quan, Y.; Liu, J. Simulation of forest fire spread based on artificial intelligence. *Ecol. Indic.* **2022**, *136*, 108653. [CrossRef]
56. Loboda, T.; O'neal, K.J.; Csiszar, I. Regionally adaptable dNBR-based algorithm for burned area mapping from MODIS data. *Remote Sens. Environ.* **2007**, *109*, 429–442. [CrossRef]
57. Li, M.; Kang, X.; Fan, W. Burned area extraction in Huzhong forests based on remote sensing and the spatial analysis of the burned severity. *Sci. Silvae Sin.* **2017**, *53*, 163–174.

58. Collins, L.; Griffioen, P.; Newell, G.; Mellor, A. The utility of Random Forests for wildfire severity mapping. *Remote Sens. Environ.* **2018**, *216*, 374–384. [CrossRef]
59. Wang, S.; Chen, W.; Xie, S.M.; Azzari, G.; Lobell, D.B. Weakly supervised deep learning for segmentation of remote sensing imagery. *Remote Sens.* **2020**, *12*, 207. [CrossRef]
60. Montandon, L.M.; Small, E.E. The impact of soil reflectance on the quantification of the green vegetation fraction from NDVI. *Remote Sens. Environ.* **2008**, *112*, 1835–1845. [CrossRef]
61. Rouse, J.W., Jr.; Haas, R.H.; Schell, J.A.; Deering, D.W. *Monitoring the Vernal Advancement and Retrogradation (Green Wave Effect) of Natural Vegetation*; (No. NASA-CR-132982); NASA: Washington, DC, USA, 1973.
62. Jaafari, A.; Termeh, S.V.R.; Bui, D.T. Genetic and firefly metaheuristic algorithms for an optimized neuro-fuzzy prediction modeling of wildfire probability. *J. Environ. Manag.* **2019**, *243*, 358–369. [CrossRef]
63. Malik, T.; Rabbani, G.; Farooq, M. Forest fire risk zonation using remote sensing and GIS technology in Kansrao Forest Range of Rajaji National Park, Uttarakhand, India. *India. Inter. J. Adv. RS GIS* **2013**, *2*, 86–95.
64. Miettinen, J.; Langner, A.; Siegert, F. Burnt area estimation for the year 2005 in Borneo using multi-resolution satellite imagery. *Int. J. Wildland Fire* **2007**, *16*, 45–53. [CrossRef]
65. Meng, R.; Wu, J.; Schwager, K.L.; Zhao, F.; Dennison, P.E.; Cook, B.D.; Brewster, K.; Green, T.M.; Serbin, S.P. Using high spatial resolution satellite imagery to map forest burn severity across spatial scales in a Pine Barrens ecosystem. *Remote Sens. Environ.* **2017**, *191*, 95–109. [CrossRef]
66. Mazuelas Benito, P.; Fernández Torralbo, A. Landsat and MODIS Images for Burned Areas Mapping in Galicia, Spain. 2012. Available online: https://www.diva-portal.org/smash/record.jsf?dswid=7937&pid=diva2%3A553135 (accessed on 13 July 2022).
67. Chuvieco, E.; Cocero, D.; Riano, D.; Martin, P.; Martınez-Vega, J.; De La Riva, J.; Pérez, F. Combining NDVI and surface temperature for the estimation of live fuel moisture content in forest fire danger rating. *Remote Sens. Environ.* **2004**, *92*, 322–331. [CrossRef]
68. Wu, Z.; He, H.S.; Yang, J.; Liu, Z.; Liang, Y. Relative effects of climatic and local factors on fire occurrence in boreal forest landscapes of northeastern China. *Sci. Total Environ.* **2014**, *493*, 472–480. [CrossRef] [PubMed]
69. Chang, Y.; Zhu, Z.; Bu, R.; Chen, H.; Feng, Y.; Li, Y.; Hu, Y.; Wang, Z. Predicting fire occurrence patterns with logistic regression in Heilongjiang Province, China. *Landsc. Ecol.* **2013**, *28*, 1989–2004. [CrossRef]
70. Guo, F.; Su, Z.; Wang, G.; Sun, L.; Tigabu, M.; Yang, X.; Hu, H. Understanding fire drivers and relative impacts in different Chinese forest ecosystems. *Sci. Total Environ.* **2017**, *605*, 411–425. [CrossRef]
71. Wu, Z.; He, H.S.; Yang, J.; Liang, Y. Defining fire environment zones in the boreal forests of northeastern China. *Sci. Total Environ.* **2015**, *518*, 106–116. [CrossRef]
72. Zhang, H.; Qi, P.; Guo, G. Improvement of fire danger modelling with geographically weighted logistic model. *Int. J. Wildland Fire* **2014**, *23*, 1130–1146. [CrossRef]
73. Pereira, M.G.; Caramelo, L.; Orozco, C.V.; Costa, R.; Tonini, M. Space-time clustering analysis performance of an aggregated dataset: The case of wildfires in Portugal. *Environ. Model. Softw.* **2015**, *72*, 239–249. [CrossRef]
74. Guo, F.; Su, Z.; Wang, G.; Sun, L.; Lin, F.; Liu, A. Wildfire ignition in the forests of southeast China: Identifying drivers and spatial distribution to predict wildfire likelihood. *Appl. Geogr.* **2016**, *66*, 12–21. [CrossRef]
75. Syphard, A.D.; Radeloff, V.C.; Keeley, J.E.; Hawbaker, T.J.; Clayton, M.K.; Stewart, S.I.; Hammer, R.B. Human influence on California fire regimes. *Ecol. Appl.* **2007**, *17*, 1388–1402. [CrossRef]
76. Pereira, M.; Malamud, B.; Trigo, R.; Alves, P. The history and characteristics of the 1980–2005 Portuguese rural fire database. *Nat. Hazards Earth Syst. Sci.* **2011**, *11*, 3343–3358. [CrossRef]
77. Zumbrunnen, T.; Pezzatti, G.B.; Menéndez, P.; Bugmann, H.; Bürgi, M.; Conedera, M. Weather and human impacts on forest fires: 100 years of fire history in two climatic regions of Switzerland. *For. Ecol. Manag.* **2011**, *261*, 2188–2199. [CrossRef]
78. Garcia, C.V.; Woodard, P.; Titus, S.; Adamowicz, W.; Lee, B. A logit model for predicting the daily occurrence of human caused forest-fires. *Int. J. Wildland Fire* **1995**, *5*, 101–111. [CrossRef]
79. Miranda, B.R.; Sturtevant, B.R.; Stewart, S.I.; Hammer, R.B. Spatial and temporal drivers of wildfire occurrence in the context of rural development in northern Wisconsin, USA. *Int. J. Wildland Fire* **2011**, *21*, 141–154. [CrossRef]
80. Barmpoutis, P.; Papaioannou, P.; Dimitropoulos, K.; Grammalidis, N. A review on early forest fire detection systems using optical remote sensing. *Sensors* **2020**, *20*, 6442. [CrossRef]
81. Mohajane, M.; Costache, R.; Karimi, F.; Pham, Q.B.; Essahlaoui, A.; Nguyen, H.; Laneve, G.; Oudija, F. Application of remote sensing and machine learning algorithms for forest fire mapping in a Mediterranean area. *Ecol. Indic.* **2021**, *129*, 107869. [CrossRef]
82. Slezakova, K.; Morais, S.; do Carmo Pereira, M. Forest fires in Northern region of Portugal: Impact on PM levels. *Atmos. Res.* **2013**, *127*, 148–153. [CrossRef]
83. Valendik, E.; Kosov, I. Effect of thermal radiation of forest fire on the environment. *Contemp. Probl. Ecol.* **2008**, *1*, 399. [CrossRef]
84. Yao, J.; Zhai, H.; Tang, X.; Gao, X.; Yang, X. Amazon Fire Monitoring and Analysis Based on Multi-source Remote Sensing Data. In *IOP Conference Series: Earth and Environmental Science*; IOP Publishing: Bristol, UK, 2020; p. 042025.